Correlation Between AO6 Polyhedral Distortion and Negative Thermal Expansion in Orthorhombic Y2Mo3O12 and Related Materials

ARTICLE *in* CHEMISTRY OF MATERIALS · JUNE 2009

Impact Factor: 8.35 · DOI: 10.1021/cm900650c

8 AUTHORS, INCLUDING:

B. A. Marinkovic
Pontifícia Universidade Católica do Rio de J…
80 PUBLICATIONS **875** CITATIONS
SEE PROFILE

Roberto Ribeiro de Avillez
Pontifícia Universidade Católica do Rio de J…
95 PUBLICATIONS **587** CITATIONS
SEE PROFILE

Fernando Rizzo
Pontifícia Universidade Católica do Rio de J…
139 PUBLICATIONS **1,561** CITATIONS
SEE PROFILE

Fabio Furlan Ferreira
Universidade Federal do ABC (UFABC)
69 PUBLICATIONS **538** CITATIONS
SEE PROFILE

2886 *Chem. Mater.* **2009,** *21,* 2886–2894
DOI:10.1021/cm900650c

CHEMISTRY OF MATERIALS
Article

Correlation between AO_6 Polyhedral Distortion and Negative Thermal Expansion in Orthorhombic $Y_2Mo_3O_{12}$ and Related Materials

Bojan A. Marinkovic,*[,†] Monica Ari[†] Roberto R. de Avillez,[†] Fernando Rizzo,[†] Fabio F. Ferreira,[‡] Kimberly J. Miller,[§] Michel B. Johnson,[§] and Mary Anne White[§]

[†]*Departamento de Ciência dos Materiais e Metallurgia, Pontifícia Universidade Católica do Rio de Janeiro (PUC-Rio), Rua Marquês de São Vicente 225, Gávea, RJ, Brasil,* [‡]*Laboratório Nacional de Luz Síncrotron (LNLS), CP 6192, CEP 13083-970, Campinas, SP, Brasil, and* [§]*Department of Chemistry and Institute for Research in Materials, Dalhousie University, Halifax, Nova Scotia B3H 4J3, Canada*

Received March 6, 2009. Revised Manuscript Received May 7, 2009

The *Pbcn* orthorhombic phase of $Y_2Mo_3O_{12}$ has been examined through high-resolution X-ray powder diffraction (10−450 K), heat capacity determination (2−390 K), and differential scanning calorimetry (103−673 K). No phase transition was found over this temperature range. The overall thermal expansion is negative, and the average linear thermal expansion coefficient, α_l, is $-9.02 \times 10^{-6}\,K^{-1}$ averaged over $T = 20$−450 K. From a thorough analysis of the structure of $Y_2Mo_3O_{12}$, we find that the YO_6 octahedra and MoO_4 tetrahedra are increasingly distorted with increasing temperature. The inherent volume distortion parameter (v) of AO_6 has been introduced to quantitatively evaluate polyhedral distortion and it is observed that this parameter is strongly correlated with the linear coefficient thermal expansion (α_l) of different members of the $A_2M_3O_{12}$ family. We attribute the negative thermal expansion to the reduction of the mean Y−Mo nonbonded distances and Y−O−Mo bond angles with increasing temperature, the joint action of high-energy optical and low-energy translational and librational modes.

1. Introduction

The possibility of controlling the coefficient of thermal expansion in pure and composite materials has been the principal driving force in the search for crystal phases with unusually low, zero, or even negative thermal expansion (NTE). The field has been growing since the rediscovery of NTE in cubic ZrW_2O_8 (AM_2O_8 family) by X-ray powder diffraction (XRPD),[1] whereas several other open-framework classes of known ceramics, such as AO_2,[2] AMO_5,[3] AM_2O_7,[4] A_2O[5] and $A_2M_3O_{12}$[6−8] have emerged as potential sources of crystal phases with low or NTE. Moreover, members of a new class of ceramics with the general chemical formula $AA'M_3O_{12}$ ($A = Mg^{2+}$; $A' = Hf^{4+}$,Zr^{4+}; $M = W^{6+}$,Mo^{6+}) with a new orthorhombic structure have been synthesized and characterized for thermal expansion, showing promising unusually low or even negative thermal expansion properties.[9−11] Generally, it is assumed that the low-energy transverse thermal vibration of the two-coordinate atoms along with possible contributions from translational modes are responsible for NTE in the open-framework orthorhombic structures. The rigid-unit mode model of NTE considers the orthorhombic structure as corner-sharing units made up of semirigid AO_6 octrahedra and MO_4 tetrahedra which expand anisotropically on heating to produce a cooperative tilting, resulting in a net negative thermal expansion. Recently, NTE was found in a metallic phase, $GdPd_3B_{0.25}C_{0.75}$, and attributed to the effect of low-energy transverse vibrational modes of two-coordinate Pd atoms.[12]

The $A_2M_3O_{12}$ family is especially attractive due to the chemical flexibility within the orthorhombic *Pbcn* (No. 60) space group that results in a large range of variation of linear coefficients of thermal expansion for the orthorhombic $A_2M_3O_{12}$ phases, from low positive to large negative values.[13−15] This feature of orthorhombic $A_2M_3O_{12}$ phases makes it possible to synthesize solid

*Corresponding author. Tel: 51-21-35271954. Fax: 51-21-35271248. E-mail: bojan@puc-rio.br.

(1) Evans, J. S. O.; Mary, T. A.; Vogt, T.; Subramanian, M. A.; Sleight, A. W. *Chem. Mater.* **1996**, *8*, 2809.
(2) Marinkovic, B. A.; Jardim, P. M.; Saavedra, A.; Lau, L. Y.; Baehtz, C.; de Avillez, R. R.; Rizzo, F. *Microporous Mesoporous Mater.* **2004**, *71*, 117.
(3) Amos, T. G.; Yokochi, A.; Sleight, A. W. *J. Solid State Chem.* **1998**, *14*, 303.
(4) Korthuis, V.; Khosrovani, N.; Sleight, A. W.; Roberts, N.; Dupree, R.; Warren, W. W.Jr. *Chem. Mater.* **1995**, *7*, 412.
(5) Kennedy, B. J.; Kubota, Y.; Kato, K. *Solid State Commun.* **2005**, *136*, 177.
(6) Evans, J. S. O.; Mary, T. A.; Sleight, A. W. *J. Solid State Chem.* **1998**, *137*, 148.
(7) Evans, J. S. O.; Mary, T. A. *Int. J. Inorg. Mater.* **2000**, *2*, 143.
(8) Gates, S. D.; Colin, J. A.; Lind, C. *J. Mater. Chem.* **2006**, *16*, 4214.
(9) Suzuki, T.; Omote, A. *J. Am. Ceram. Soc.* **2004**, *87*, 1365.
(10) Gindhart, A. M.; Lind, C.; Green, M. *J. Mater. Res.* **2008**, *23*, 210.
(11) Marinkovic, B. A.; Jardim, P. M.; Ari, M.; de Avillez, R. R.; Rizzo, F.; Ferreira, F. F. *Phys. Status Solidi (b)* **2008**, *245*, 2514.
(12) Pandey, A.; Mazumdar, C; Ranganathan, R.; Tripathi, S.; Pandey, D.; Dattagupta, S. *Appl. Phys. Lett.* **2008**, *92*, 261913.
(13) Wu, M. M.; Peng, J.; Cheng, Y. Z.; Wang, H; Yu, Z. X.; Chen, D. F.; Hu, Z. B. *Solid State Sci.* **2006**, *8*, 665.
(14) Sumithra, S.; Umarji, A. M. *Solid State Sci.* **2004**, *6*, 1313.
(15) Ari, M.; Jardim, P. M.; Marinkovic, B. A.; Rizzo, F.; Ferreira, F. F. *J. Solid State Chem.* **2008**, *181*, 1472.

 Published on Web 06/04/2009

solutions with controlled coefficients of thermal expansion. Another important characteristic of the $A_2M_3O_{12}$ family is the existence of an orthorhombic-to-monoclinic phase transition,[16] because low-temperature monoclinic counterparts of the orthorhombic phases have very different thermal expansion properties and their linear coefficients of thermal expansion are highly positive.[7,17] Some authors have shown a correlation between the temperature of the phase transition (T_t) in this family and electronegativity of A,[16,17] with more electronegative A atoms exhibiting higher phase transition temperatures (see Table S1 of the Supporting Information for a summary of the measured T_t for all known members of $A_2M_3O_{12}$ family). Several potential applications of NTE materials, such as in Fiber Bragg gratings, require that materials show NTE at room temperature. Rare earth $A_2M_3O_{12}$ phases are the natural candidates for these purposes because their orthorhombic NTE phases are generally thermodynamically or kinetically stable at near room temperature.

The thermal expansion and phase transition of the orthorhombic $Y_2Mo_3O_{12}$ phase (with *Pbcn* space group) were recently studied for the first time, and it was observed that this phase presents very high NTE between 403 and 1073 K.[18] Note that at temperatures lower than 823 K this phase is metastable (another orthorhombic phase with *Pba*2 space group is stable), but it is kinetically preferred.[19] However, the *Pbcn* phase is hygroscopic and poorly crystalline in air at room temperature; therefore, it needs to be thermally treated to assume its anhydrous crystalline orthorhombic (*Pbcn*) NTE form. This is especially important because the presence of water hinders the motions of the polyhedra.[20]

There is little information about the orthorhombic *Pbcn* $Y_2Mo_3O_{12}$ phase below room temperature. Therefore, the aim of this study was to shed more light on thermal expansion, heat capacity and possible phase transitions of orthorhombic (*Pbcn*) $Y_2Mo_3O_{12}$ in the temperature range between 2 and 450 K.

2. Experimental Methods

$Y_2Mo_3O_{12}$ was produced by the solid-state reaction of a stoichiometric mixture of MoO_3 (Fluka 99.98%) and Y_2O_3 (Labosi 99.9%). The reactants were preheated at 773 K in air for three hours, then weighed, mixed and homogenized in agate mortar. The preheated powders were heat treated in air in alumina crucibles at 973 K for 48 h with intermediate grinding and then 1053 K for 20 h, followed by cool down in the furnace.

$Y_2Mo_3O_{12}$ is highly hygroscopic.[18,19] To make $Y_2Mo_3O_{12}$ water-free, the following procedure was adopted prior to the collection of high-resolution X-ray powder diffraction (HRXRPD) data. The $Y_2Mo_3O_{12}$ sample was introduced into a commercial closed-cycle He cryostat (Advanced Research Systems) at room temperature. After that, an HRXRPD pattern was taken prior to heat treatment, showing a poorly crystalline phase, indicative of the hydrate.[18] The temperature was then raised to 450 K under a vacuum (8−10 mTorr), and the sample was left for 1 h at this temperature. An HRXRPD was carried out after this, showing a highly crystalline pattern.[18] The sample was then cooled in situ to 10 K and slowly heated to 20 K.

HRXRPD data were collected, in a vacuum (8−10 mTorr), at four different temperatures (20, 150, 300, and 450 K), using a commercial closed-cycle He cryostat, with vibration damping and temperature control (10 to 450 K), at the X-ray Powder Diffraction (D10B-XPD) beamline[21] of the Brazilian Synchrotron Light Laboratory (LNLS). X-rays of 1.23989 Å wavelength were selected by a double-bounced Si(111) monochromator with water refrigeration in the first crystal, whereas the second one is bent for sagittal focusing. The beam was vertically focused in the sample's position on a spot of ~1 mm (vertical) × ~2 mm (horizontal). The experiments were performed in the vertical scattering plane, i.e., perpendicular to the linear polarization of the incident photons. Values of the X-ray wavelength used in this study and the zero-point displacement were determined from several reflections of an external SRM640c Si standard. The diffracted beam was analyzed using a Ge(111) single crystal and detected using a NaI(Tl) scintillation counter with a pulse-height discriminator in the counting chain. The incoming beam also was monitored by a scintillation counter to normalize the decay of the primary beam. Data were recorded at different temperatures for 2 s at each 2θ in steps of 0.004° from 10 to 80°.

Rietveld refinement was performed using Topas-Academic software.[22] Analysis of polyhedral distortion was carried out using the IVTON program.[23]

Thermal measurements required consolidated samples. Because of the hygroscopic nature of the compound and the poor mechanical stability of samples as prepared, all samples were loaded into a press and the entire assembly was preheated in an oven at 423 K for at least one hour prior to forming the pellet. The assembly was then removed from the oven and ~0.5 GPa of pressure was applied using a Carver Laboratory Press, model C (from Fred S. Carver, Inc.). The assembly was allowed to cool until tactable and the pellet was removed and split into smaller portions. The pellet fragments were sorted and one or two samples were selected based on size, shape, and mechanical integrity. All samples were stored in a vacuum desiccator or in an oven until needed.

To determine the sample's water content after various treatments, a TA Instruments TGA Q600 was used. After the samples were heated to 403 K for 4 min in an aluminum pan under argon, the water was fully removed (limit of detection, 0.1 mol % water). Subsequent runs indicated that holding at 373 K for 10 min also was acceptable for drying the samples.

A TA Instruments Q200 series Differential Scanning Calorimeter (DSC) equipped with an LNCS cooling head and a helium atmosphere was used to investigate the presence of any thermal anomalies in anhydrous $Y_2Mo_3O_{12}$ from 103 to 673 K following preheating at 403 K. Typical sample mass was 4 mg.

Heat capacity was determined over the temperature range 2 to 390 K, using a commercial relaxation calorimeter (Physical Property Measurement System model 6000 from Quantum Design). Measurements were conducted on three anhydrous

(16) Sleight, A. W.; Brixner, L. H. *J. Solid State Chem.* **1973**, *7*, 172.
(17) Evans, J. S. O.; Mary, T. A.; Sleight, A. W. *J. Solid State Chem.* **1997**, *133*, 580.
(18) Marinkovic, B. A.; Jardim, P. M.; de Avillez, R. R.; Rizzo, F. *Solid State Sci.* **2005**, *7*, 1377.
(19) Gates, S. D.; Lind, C. *J. Solid State Chem.* **2007**, *180*, 3510.
(20) Liang, E.; Huo, H.; Wang, J.; Chao, M. *J. Phys. Chem. C* **2008**, *112*, 6577.
(21) Ferreira, F. F.; Granado, E.; Carvalho, W.Jr.; Kycia, S. W.; Bruno, D.; Droppa, R.Jr. *J. Synchrotron Radiat.* **2006**, *13*, 46.
(22) Coelho, A. A.Topas - Academic, Technical Reference, **2004**.
(23) Balic Zunic, T.; Vickovic, I. *J. Appl. Crystallogr.* **1996**, *29*, 305.

samples of $Y_2Mo_3O_{12}$ ranging in mass from 4.949 mg to 13.940 mg. Because of the hygroscopic nature of the samples and the limitations presented by the thermal-contact greases available, separate low-temperature and high-temperature methods needed to be developed in order to obtain meaningful data. Typically, Apiezon N grease is used to ensure thermal contact between the sample and the platform because of its excellent heat transfer properties down to 2 K, and accurate heat capacity data usually can be obtained with this method.[24] However, this hygroscopic sample required final drying at high temperature in situ prior to the heat capacity measurements, and Apiezon N grease melts (and loses thermal contact) at 320 K. Therefore, Apiezon T grease was used since it has a higher melting point (403 K). The sample was preheated in the PPMS at 320 K for 6 h under high vacuum. (Separate experiments showed that this was long enough and high enough in temperature to remove water.) Data were collected with Apiezon T grease from 2 to 225 K. At higher temperatures, Apiezon T was found to creep into the sample, reducing thermal contact. Therefore, Apiezon H grease was used for data collected in the range 390 to 210 K. However, H could not be used at lower temperatures because it loses contact with the sample at temperatures below 200 K.

A scanning electron microscope (SEM) Zeiss DSM 960 equipped with an X-ray energy-dispersive spectrometer (EDS) was used in order to verify the phase composition of the synthesized samples.

3. Results

The $Y_2Mo_3O_{12}$ sample investigated by HRXRPD was single-phased over the temperature range 10 to 450 K and no traces of the precursor phases or other compounds having different compositions were found. SEM analysis of this sample in backscattering mode corroborated this finding. Considering that the monoclinic and orthorhombic phases of compounds in the $A_2M_3O_{12}$ family have rather similar diffraction patterns, a 2θ range of 16−18°, where the major differences between the two structures are observed, was systematically measured to follow any possible phase transition from the orthorhombic to monoclinic structure. We found, surprisingly, that no first-order phase transition occurred in the investigated range (10 to 450 K). The absence of an orthorhombic-to-monoclinic phase transition for $Y_2Mo_3O_{12}$ was confirmed through Rietveld refinement of the whole diffraction pattern (Figure 1). Therefore, the $Y_2Mo_3O_{12}$ phase maintained the orthorhombic *Pbcn* structure from 450 K to at least 20K.

Figure 2 shows the DSC results for anhydrous $Y_2Mo_3O_{12}$. Within the limit of detection (about 1 J g^{-1}), there are no features in the temperature range from 103 to 673 K. The heat capacity results (Figure 3; table in the Supporting Information) show no thermal anomalies over the examined temperature range 2−390 K. Furthermore, the heat capacity shows no dependence on sample mass over the range 4.9491 mg to 13.9403 mg. (Sample mass dependence can be indicative of low thermal conductivity, leading to uncertainty in results).[24] Taking into account the full temperature range of the DSC and heat capacity results, we find no thermal anomalies in $Y_2Mo_3O_{12}$ over the temperature range 2 to 673 K, again supporting the absence of an orthorhombic-to-monoclinic transition.

The variation of unit-cell parameters of $Y_2Mo_3O_{12}$ in the range 20 to 450 K is shown in Figure 4. The *b*- and *c*-axes diminish with increasing temperature throughout

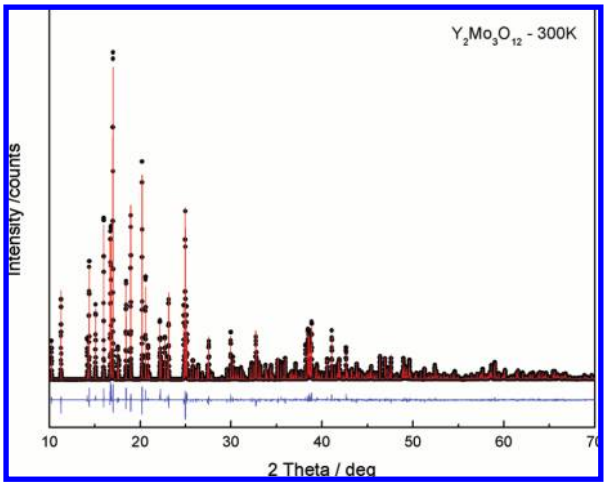

Figure 1. High-resolution XRPD pattern for $Y_2Mo_3O_{12}$ at $T = 300$ K. Experimental profile (points) and calculated and difference profiles (full lines).

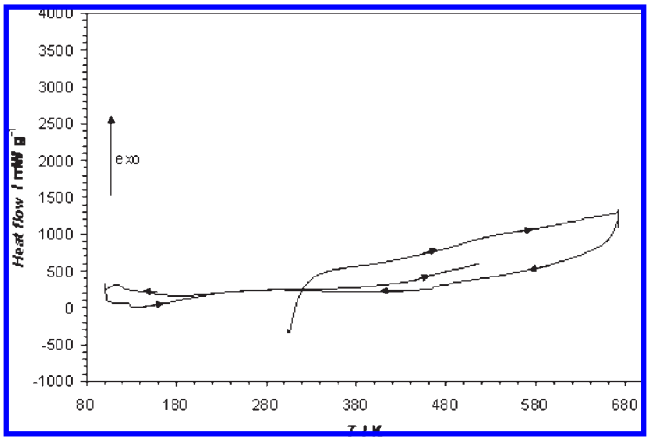

Figure 2. Differential scanning calorimetry (DSC) results for 4.826 mg of anhydrous $Y_2Mo_3O_{12}$ measured in a helium atmosphere from 103 to 673K. The arrows indicate the direction of the scan, starting at room temperature.

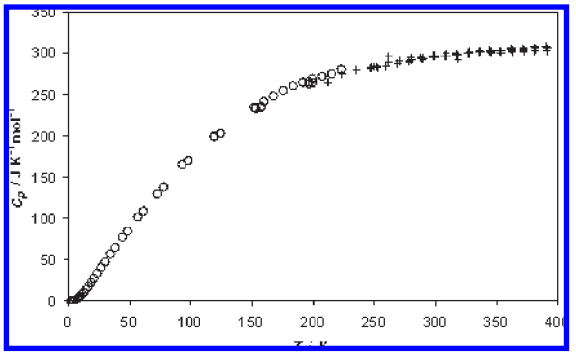

Figure 3. Heat capacity results for $Y_2Mo_3O_{12}$ over the temperature range 2 to 390 K. ○, measurements with Apiezon T; +, measurements with Apiezon H.

(24) Kennedy, C. A.; Stancescu, M.; Marriott, R. A.; White, M. A. *Cryogenics* **2007**, *47*, 107.

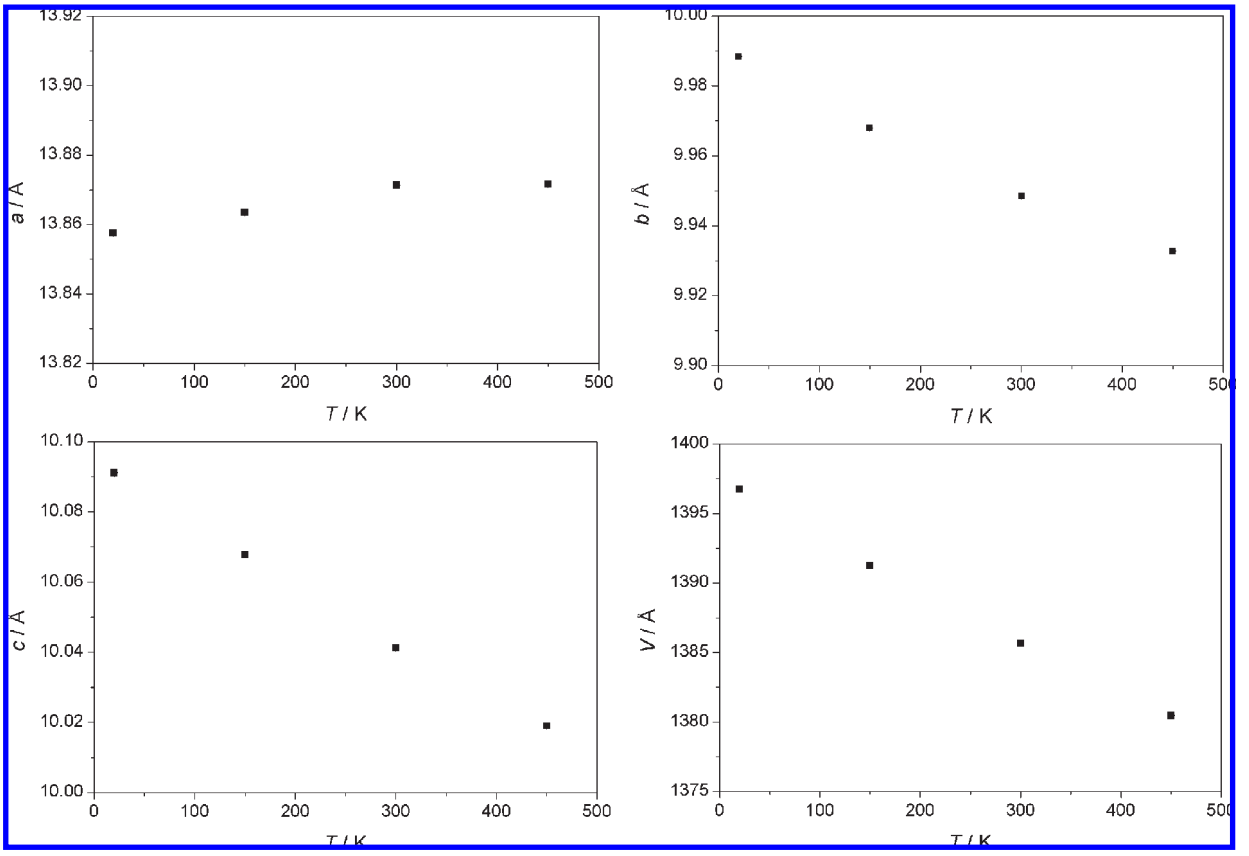

Figure 4. Lattice parameters of $Y_2Mo_3O_{12}$ as a function of temperature. Standard uncertainties are included but are too small to appear in the graphs.

the temperature range. On the other hand, the *a*-axis increases from 20 to 300 K, but then remains unchanged between 300 and 450 K. This behavior of the cell parameters leads to a nearly linear reduction of the cell volume as a function of temperature. The net volume coefficient of thermal expansion, α_V, of $Y_2Mo_3O_{12}$ in the range 20 to 450 K was highly negative, -2.71×10^{-5} K^{-1}, giving a linear coefficient of expansion, α_l ($= \alpha_V/3$) of -9.02×10^{-6} K^{-1} averaged over this temperature range.

Atomic positions and isotropic displacement factors for 20, 300, and 450 K, adjusted through the Rietveld method, are supplied in the Supporting Information and deposited in the Inorganic Crystal Structure Database (ICSD), codes 420151, 420152, and 420153, respectively (because of some technical problems during data acquiring at $T = 150$ K, the corresponding HRXRPD data were not of sufficient quality to be successfully treated by the Rietveld method). Table 1 summarizes the Rietveld reliability factors for the refined diffraction patterns, and an example of the Rietveld refined diffraction pattern ($T = 300$ K) is shown in Figure 1. All other refined diffraction patterns are supplied in the Supporting Information. Isotropic displacement parameters for Y, Mo1, Mo2, and O plotted versus temperature (see the Supporting Information) demonstrate smooth (linear) relationships (linear regression *R*-factor higher than 99.7% in all cases) corroborating that a reliable structural model free of systematic errors was refined through the Rietveld method.[6]

Table 1. Rietveld Reliability Factors for the Refined Diffraction Patterns of $Y_2Mo_3O_{12}$

T (K)	R_{Bragg} (%)*	GOF	R_{wp} (%)	R_{exp} (%)
20	4.41	2.86	13.48	9.55
300	4.06	2.64	13.27	9.89
450	4.78	2.47	14.01	10.46

* $R_B = (\Sigma_{hkl}I_{\text{"O"},hkl} - I_{C,hkl})/(\Sigma_{hkl}I_{\text{"O"},hkl})$, where $I_{\text{"O"}}$ and I_C are the "observed" and calculated intensities of the *hkl* reflection.

Internal angles of the polyhedra, YO_6, $Mo1O_4$, and $Mo2O_4$, as a function of temperature are presented in Figure 5. Idealized 90° octahedral angles over the investigated temperature interval ranged from 85.07° (O5−Y−O1, 300 K) to 95.19° (O3−Y−O4, 20 K). The maximum angular variation of an internal 90° bond angle is 1.95° for O6−Y−O1, whereas the average variation of 12 YO_6 90° bond angles is 1.23°. $Mo1O_4$ tetrahedral bond angles ranged from 105.66° (O4−Mo1−O2, 450 K) to 113.07° (O4−Mo1−O4, 450 K), whereas $Mo2O_4$ tetrahedral bond angles ranged from 107.46° (O1−Mo2−O5, 20 K) to 111.47° (O1−Mo2−O6, 20 K). The maximum variation in $Mo1O_4$ tetrahedra was observed for the O4−Mo1−O2 angle (4.89°), whereas the average variation of internal angles with temperature in the $Mo1O_4$ tetrahedron was 3.23°. In the $Mo2O_4$ tetrahedron, the maximum variation was observed for the O1−Mo2−O6 angle (3.57°), whereas the average variation of internal angles with temperature was 1.63°. The apparent average Y−O distance showed a slight negative variation with temperature [d_{av}(Y−O, in Å)$= 2.27860 - 2.05388 \times 10^{-5}$ T]

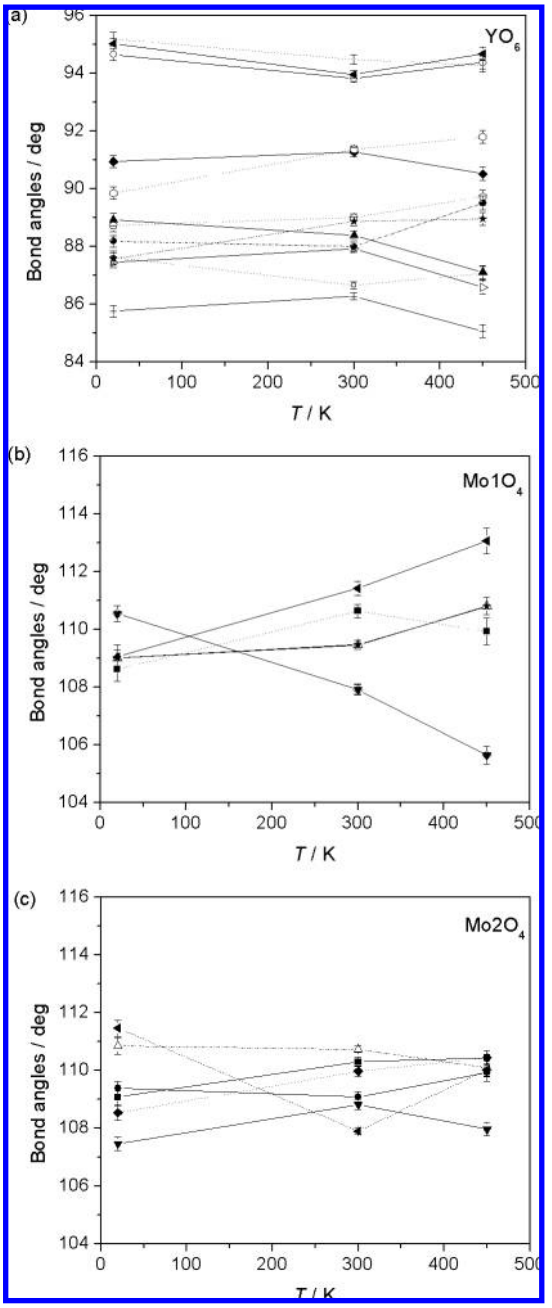

Figure 5. Temperature dependence of internal polyhedral angles in $Y_2Mo_3O_{12}$ for (a) YO_6, (b) $Mo1O_4$, and (c) $Mo2O_4$. Uncertainties are esd's and lines are to guide the eye.

within the investigated temperature range (Figure 6a), as did the average Mo−O distance [d_{av}(Mo−O, in Å) = $1.72101 - 2.21134 \times 10^{-5}T$] (Figure 6b).

The distortion of the polyhedra (YO_6, $Mo1O_4$ and $Mo2O_4$) in $Y_2Mo_3O_{12}$ was expressed through the volume distortion parameter (υ) proposed by Makovicky and Balic-Zunic,[25] $\upsilon = (V_i - V_r)/V_i$, where V_i is the volume of the ideal polyhedron and V_r is the volume of the real polyhedron. Figure 7 summarizes the variations of the volume distortion parameter for the three types of polyhedra in $Y_2Mo_3O_{12}$ with temperature.

(25) Makovicky, E.; Balic-Zunic, T. *Acta Crystallogr., Sect. B* **1998**, *54*, 766.

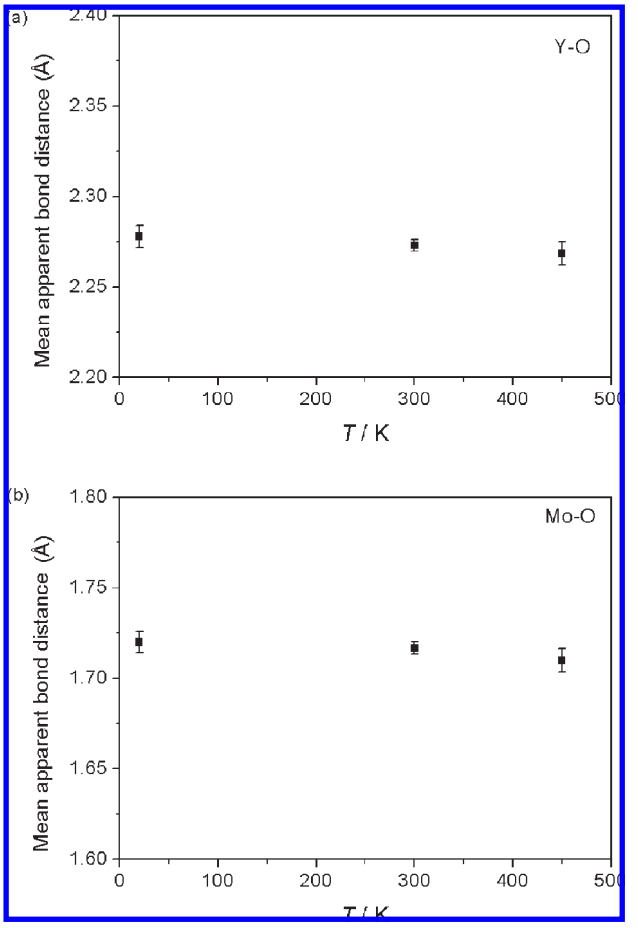

Figure 6. Bond distances as a function of temperature in $Y_2Mo_3O_{12}$: (a) mean apparent Y−O bond distances, (b) mean apparent Mo−O bond distances.

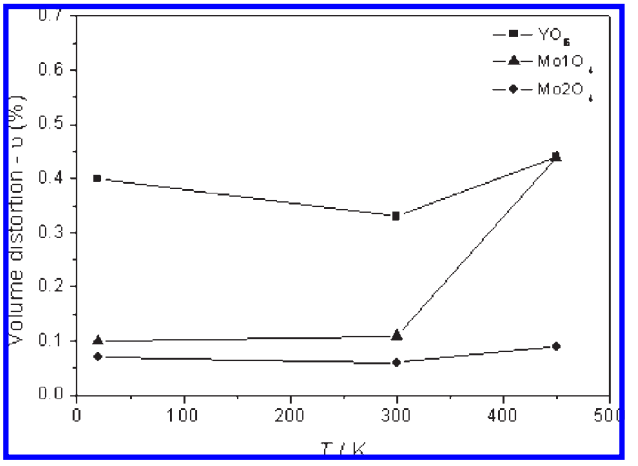

Figure 7. Polyhedral volume distortion (υ) of YO_6, $Mo1O_4$, and $Mo2O_4$ in $Y_2Mo_3O_{12}$ as a function of temperature. Lines are to guide the eye.

The average nonbonded Y−Mo distances as a function of temperature show a significant reduction, from 3.9140 (13) Å at T = 20 K to 3.8966(13) Å at T = 450 K (Figure 8a). The average interpolyhedral Y−O−Mo angle also shows a reduction as a function of temperature (Figure 8b). The bond valences of the ions in $Y_2Mo_3O_{12}$ have been calculated through the bond-valence sum approach[26] and are plotted in Figure 9. Calculated bond

(26) Brown, I. D.; Altermatt, D. *Acta Crystallogr., Sect. B* **1985**, *41*, 244.

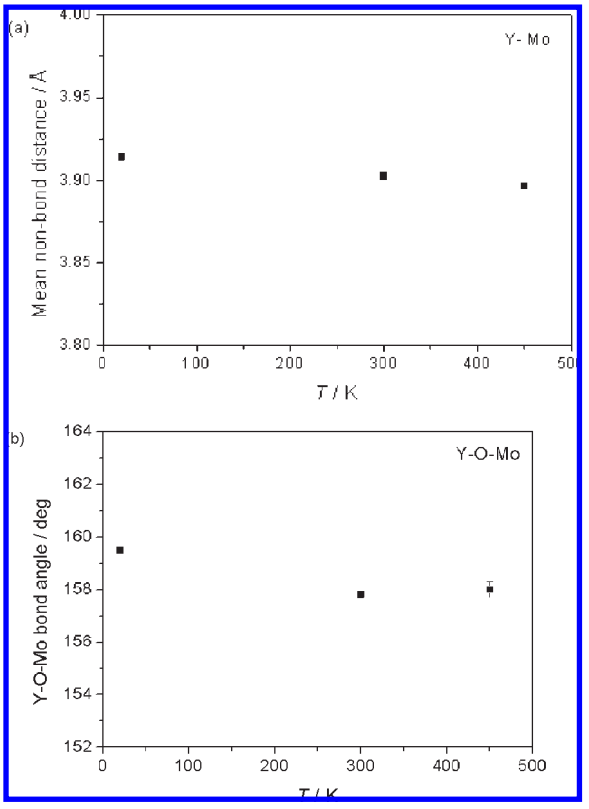

Figure 8. Nonbonded parameters in $Y_2Mo_3O_{12}$ as a function of temperature. (a) Mean nonbonded Y−Mo distances and (b) Y−O−Mo bond angles. Standard uncertainties are included but are too small to appear in part a.

valences (Figure 9) are within the acceptable range to validate the refined crystal structure, although the values for Mo1 and Mo2 were higher than expected. Similar bond valence features were observed for $Y_2W_3O_{12}$ (see the Supporting Information) based on structural data presented elsewhere.[27] Slightly overbonded Mo cations in this structure might be a consequence of compressive stresses in the Mo−O bonds resulting in metastability[28] in orthorhombic *Pbcn* $Y_2Mo_3O_{12}$.[19]

4. Discussion

The temperature of orthorhombic-to-monoclinic phase transition in several $A_2M_3O_{12}$ compounds has been correlated to the electronegativities of the A atoms.[17] The concept is that as the electronegativity of the A atom increases, the electron density on the bridging oxygen atoms should decrease, causing the oxygen−oxygen attraction to increase, leading to structural transition at higher temperatures. However, the structure is very ionic (Figure 9) and the correlation was with the electronegativity of the neutral atoms[29] (although referred to as that of A^{3+} ions).[17] Correlation of the orthorhombic-to-monoclinic phase transition temperature of compounds in the $A_2M_3O_{12}$ family with the electronegativities of the A^{3+} ions[30] (see the Supporting Information) is not as

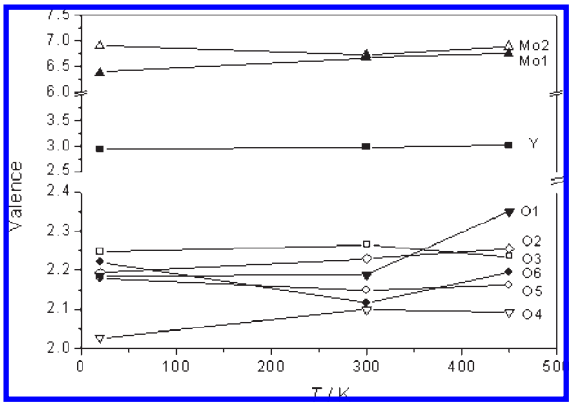

Figure 9. Calculated valences for Y^{3+}, Mo^{6+}, and O^{2-} as functions of temperature for $Y_2Mo_3O_{12}$: Y (■), Mo1 (▲), Mo2 (Δ), O1 (▼), O2 (◊), O3 (□), O4 (▽), O5 (○), and O6 (•). Lines are to guide the eye.

strong, and cannot reliably predict whether or not there would be an orthorhombic-to-monoclinic phase transition in $Y_2Mo_3O_{12}$. There is no such transition in $Y_2W_3O_{12}$ over the temperature range 15 to 1373 K.[27] In $Sc_2Mo_3O_{12}$ this transition occurs at $T = 178$ K,[7] whereas it is absent in the tungstate counterpart[6] suggesting that in the phases where A^{3+} cations are the same, M^{6+} might play a role. It is also not clear why some other molybdates have higher temperatures of phase transition than their tungstate counterparts (for example, $In_2Mo_3O_{12}$/$In_2W_3O_{12}$),[31] as shown in the Supporting Information.

The nature of the *a*-axis variation with temperature (Figure 4a) possibly could be a sign of subtle changes. For example, $Y_2Mo_3O_{12}$ and related $A_2M_3O_{12}$ materials could be candidates for cationic migration.[32] This feature in the temperature dependence of the *a*-axis of $Y_2Mo_3O_{12}$ is unexpected and was not previously explicitly discussed in the literature, although Forster and Sleight[27] showed (see Figure 1 in ref 27) that the slope of the *a*-axis of $Y_2W_3O_{12}$ (*b*-axis in the nonstandard *Pnca* space group) changes sign, from positive to negative, at a temperature higher than 295 K. The alteration of sign of the *a*-axis thermal expansion in $Y_2Mo_3O_{12}$ was not followed by a change in the space group symmetry, whereas a slight change in negative coefficient of thermal expansion at 430 K in ZrW_2O_8 is accompanied by a phase transition from $P2_13$ to $Pa-3$.[1] If the observed temperature-dependence of the *a*-axis were a consequence of a second-order phase transition, it would be accompanied by other anomalies, but the heat capacity (Figure 3) shows no evidence of even a subtle second-order phase transition in $Y_2Mo_3O_{12}$.

To ascertain whether some subtle structural changes were taking place in $Y_2Mo_3O_{12}$, we made a thorough study of other factors. Additional Rietveld refinement efforts to reach a consistent and reliable disordered structure at 450 K (a temperature above the point where *a*-axis thermal expansion changes its sign), with Y^{3+} and/or Mo^{6+} partially occupying the nonframework tetrahedral sites, because $A_2M_3O_{12}$ is a garnet-related

(27) Forster, P. M.; Sleight, A. W. *Int. J. Inorg. Mater.* **1999**, *1*, 123.
(28) Nassif, V.; Carbonio, R. E.; Alonso, J. A. *J. Solid State Chem.* **1999**, *146*, 266.
(29) Allred, A. L.; Rochow, E. G. *J. Inorg. Nucl. Chem.* **1958**, *5*, 264.
(30) Li, K.; Xue, D. *J. Phys. Chem. A* **2006**, *110*, 11332.
(31) Sivasubramanian, V.; Ravindran, T. R.; Nithya, R.; Arora, A. K. *J. Appl. Phys.* **2004**, *96*, 387.
(32) Kohler, J.; Imanaka, N.; Adachi, G. *Chem. Mater.* **1998**, *10*, 3790.

structure in which the large cations are missing,[33] were frustrated by the tendency of atoms to assume the ordered structural form, i.e., the atomic positions presented in the Supporting Information for 450 K. Simulated annealing[34] was performed, using the Topas-Academic v4.1 software program,[22] by allowing Y^{3+} and Mo^{6+} ions to partially assume other general positions, different from the ordered structure positions reported in the Supporting Information. However, this approach did not offer a new general position for either Y^{3+} or Mo^{6+}.

Possibly, the change in sign of thermal expansion along the *a*-axis is promoted by a mechanism similar to that recently proposed[35] for cubic Cu_2O, which changes its thermal expansion from negative to positive near room temperature.[36,37] This change of thermal expansion in Cu_2O is not attributed to a phase transition, but related to the subtle competition between the two contributions, different at the atomic level, to the thermal behavior in solids.[35,36] These competing interactions in Cu_2O are the asymmetrical potential between the first neighbors, responsible for positive thermal expansion, and the transversal vibration of two-coordinate atoms (a low-energy soft vibrational mode), responsible for negative thermal expansion. The change of the sign of thermal expansion along the *a*-axis in $Y_2Mo_3O_{12}$ can be understood as a change in balance of two different contributions to thermal expansion between 300 and 450 K. Taking into account the recent findings of Liang et al.,[20] there are both high-energy optical phonons contributing to NTE in $Y_2Mo_3O_{12}$, together with the well-known low-energy (soft) modes (translational and librational motions). We propose that temperature-dependence of the contributions of these modes to NTE, relative to the positive thermal expansion contributions, provokes the change of the sign in thermal expansion along the *a*-axis, from positive to negative (i.e., the addition of high-energy modes tips the balance to NTE at higher temperatures). It is worth mentioning that this kind of change in the *a*-axis thermal expansion never occurs for the members of $A_2M_3O_{12}$ with lower NTE, such as $Sc_2W_3O_{12}$[6] and $Sc_2Mo_3O_{12}$,[7] this axis being positive over the whole temperature range. On the other hand, low-energy translational and librational modes predominate over positive thermal expansion contributions along the *b*- and *c*-axes in $Y_2Mo_3O_{12}$ already from the lowest temperatures. It is worth mentioning that the weighting of the soft mode over the positive thermal contribution has been used earlier by Smith and White[38] to explain the negative thermal expansion of Ge and several III−V and II−VI compounds below 80 K. The same mechanism explains the switch from negative thermal expansion at low temperatures to positive thermal expansion at higher temperatures in Si and CuCl.[39] We emphasize that no phase transition was involved in the change of the sign of thermal expansion in these phases.

The details of the mechanism that promotes NTE in $A_2M_3O_{12}$ were not as well understood as for the AM_2O_8 family,[40,41] until recently.[20] It had been generally assumed for $A_2M_3O_{12}$ that transverse low-energy phonon modes of two-coordinate oxygens are responsible for this phenomenon, while their polyhedra are quasi-rigid, whereas in AM_2O_8 the polyhedra are fully rigid. Also, it was generally assumed that AO_6 and MO_4 polyhedra in $A_2M_3O_{12}$ are inherently distorted in order to make a framework connected via vertices. However, these assumptions have never been quantitatively evaluated at the structural level, although it has been strongly suggested that stretching and bending modes (high-energy optical phonons) of MoO_4 tetrahedra contribute to NTE.[20] We have carried out here calculations of polyhedra distortion through the volume distortion parameter (v) as proposed by Makovicky and Balic-Zunic.[25] This parameter quantifies the regularity of the ligand distribution in the polyhedra, taking into account both the internal bond angles of polyhedra (Figure 5) and the central atom to ligand bond lengths. Therefore, v is more indicative of polyhedral distortion than just the variation of internal polyhedra bond angles. Figure 7 summarizes the temperature evolution of v for the polyhedra (YO_6, $Mo1O_4$ and $Mo2O_4$) within the $Y_2Mo_3O_{12}$ structure. The polyhedra in $Y_2Mo_3O_{12}$ have small inherent distortion at 20 K, v of ~0.4% for YO_6 and ~0.1% for both MoO_4 tetrahedra. For comparison, ZrO_6 in α-ZrW_2O_8 (low-temperature form) has v of 19.75% at 0.3 K (see the Supporting Information for more details), as calculated from literature data.[1] In $Y_2Mo_3O_{12}$, the YO_6 polyhedra are intrinsically more distorted than the two MoO_4 polyhedra. For comparison, v was also calculated for other members of the $A_2M_3O_{12}$ family where atomic coordinates at different temperatures were available in the literature ($Sc_2W_3O_{12}$, $Cr_2Mo_3O_{12}$, $Y_2W_3O_{12}$ and $Al_2W_3O_{12}$);[6,15,27,42] see Figures 10, 11 and 12.

An interesting correlation exists between v of AO_6 polyhedra in $A_2M_3O_{12}$ structures determined at the lowest available temperature (denoted inherent volume distortion parameter), and their linear thermal expansion coefficient, as shown in Figure 13: NTE increases with the increase of inherent volume distortion parameter (v) of AO_6. This correlation can be seen as a more quantitative expression of the earlier rationalization that NTE in $A_2M_3O_{12}$ increases with increase of A^{3+} radius, which promotes more distortion in AO_6.[43] It seems that this new

(33) Plyasova, L. M.; Borisov, S. V.; Belov, N. V. *Sov. Physics-Crystallography* **1967**, *12*, 25.
(34) Deem, M. W.; Newsam, J. M. *J. Am. Chem. Soc.* **1992**, *114*, 7189.
(35) Artioli, G.; Dapiaggi, M.; Fornasini, P.; Sanson, A.; Rocca, F.; Merli, M. *J. Phys. Chem. Solids* **2006**, *67*, 1918.
(36) Schäfer, W.; Kirfel, A. *Appl. Phys. A: Mater. Sci. Process.* **2002**, *74*, S1010.
(37) White, G. K. *J. Phys. C: Solid State Phys.* **1978**, *11*, 2171.
(38) Smith, T. F.; White, G. K. *J. Phys. C: Solid State Phys.* **1975**, *8*, 2031.
(39) White, G. K. *Contemp. Phys.* **1993**, *34*, 193.
(40) Mittal, R.; Chaplot, S. L.; Schober, H.; Kolesnikov, A. I.; Loong, C. K.; Lind, C.; Wilkinson, A. P. *Phys. Rev. B* **2004**, *70*, 214303.
(41) Liang, E. J.; Liang, Y.; Zhao, Y.; Liu, J.; Jiang, Y. *J. Phys. Chem. A* **2008**, *112*, 12582.
(42) Woodcock, D. A.; Lightfoot, P.; Ritter, C. *J. Solid State Chem.* **2000**, *149*, 92.
(43) Forster, P. M.; Yokochi, A.; Sleight, A. W. *J. Solid State Chem.* **1998**, *140*, 157.

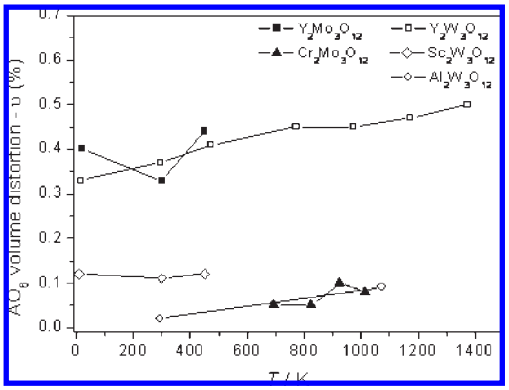

Figure 10. Volume distortion parameter (υ) of AO_6 polyhedral as a function of temperature for $A_2M_3O_{12}$ family (A = Sc, Y, Cr, Al and M = Mo, W).

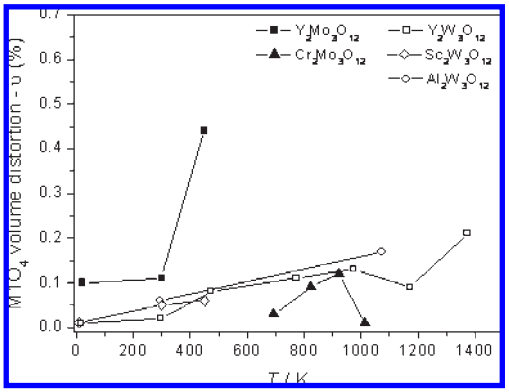

Figure 11. Volume distortion parameter (υ) of $M1O_4$ polyhedral as a function of temperature for the $A_2M_3O_{12}$ family (A = Sc, Y, Cr, Al and M = Mo, W).

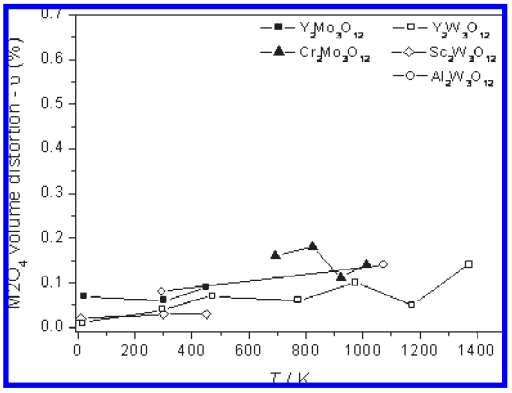

Figure 12. Volume distortion parameter (υ) of $M2O_4$ polyhedral as a function of temperature for $A_2M_3O_{12}$ family (A = Sc, Y, Cr, Al and M = Mo, W).

correlation is more robust and can provide more insight into understanding NTE in the $A_2M_3O_{12}$ family. For example, it was demonstrated by several authors[18,44] and reconfirmed in the present study that α_l is more negative for $Y_2Mo_3O_{12}$ than $Y_2W_3O_{12}$ (see Figure 5 in ref 15.). Thus, using inherent volume distortion parameter (υ) for YO_6, one can understand the difference in NTE between $Y_2Mo_3O_{12}$ and $Y_2W_3O_{12}$ (Figure 13), because υ is higher for the YO_6 polyhedra in $Y_2Mo_3O_{12}$ than in $Y_2W_3O_{12}$. The difference in thermal expansion

(44) Sumithra, S.; Umarji, A. M. *Solid State Sci.* **2006**, *8*, 1453.

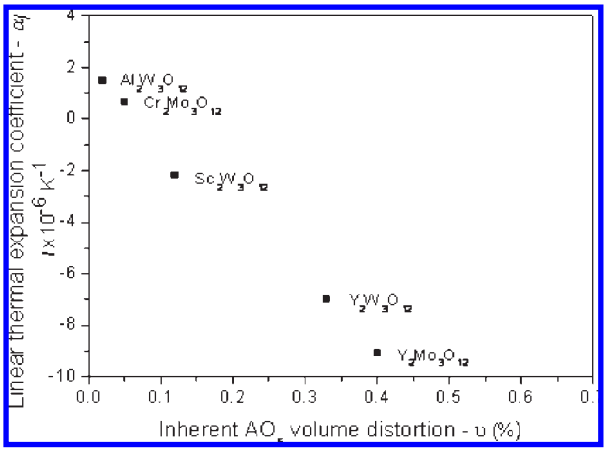

Figure 13. Average linear coefficient thermal expansion (α_l) as a function of inherent AO_6 volume distortion parameter (υ). For analyzed temperature range, see the Supporting Information.

cannot be explained by the difference in A^{3+} radii, as proposed in the earlier rationalization. Another factor that could additionally contribute to the difference in NTE between $Y_2Mo_3O_{12}$ and $Y_2W_3O_{12}$ is a greater distortion of the MoO_4 tetrahedra compared with the more regular WO_4 tetrahedra (Figures 11 and 12).

The variation of υ with temperature (Figures 10−12), provides quantitative insight concerning the rigidity of AO_6 and MO_4 polyhedra. For comparison, υ of ZrO_6 in α-ZrW_2O_8 was calculated for the whole range of its existence (see the Supporting Information) based on data reported elsewhere[1] and it was confirmed that its polyhedra are completely rigid, i.e., υ is essentially unchanged at 19.75% over the whole temperature interval. On the other hand, υ of AO_6 and MO_4 polyhedra increase with temperature for most of the members of the $A_2M_3O_{12}$ family. In $Y_2Mo_3O_{12}$, υ of YO_6 increases from 0.40% at 20 K to 0.44% at 450 K (Figure 7). Over the same temperature range, $Mo1O_4$ shows a pronounced increase of distortion with increasing temperature, while the increase in distortion for $Mo2O_4$ was milder (Figure 7). Therefore, it can be inferred that the polyhedra in $Y_2Mo_3O_{12}$ are softer than in ZrW_2O_8. The most illustrative example of this tendency in the $A_2M_3O_{12}$ family is $Y_2W_3O_{12}$, for which diffraction data are available over the largest temperature interval (15 to 1373 K).[27] Over this temperature range, υ of YO_6 increased by a factor of 1.5 (Figure 10), whereas the relative increase of this parameter for $Mo1O_4$ (Figure 11) was even higher. The $Mo2O_4$ distortion also significantly increased with temperature (Figure 12). In all members of the $A_2Mo_3O_{12}$ family that have been examined, the $Mo2O_4$ tetrahedra are more regular and more rigid than $Mo1O_4$.

Mean apparent Y−O and Mo−O bond lengths in $Y_2Mo_3O_{12}$ showed slight decreases from 20 to 450 K (Figure 6). This feature of Y−O and Mo−O bond lengths is expected for the structures with correlated motion of atoms[45] such as $A_2M_3O_{12}$,[46] and has been explained by

(45) Busing, W. R.; Levy, H. A. *Acta Crystallogr.* **1964**, *17*, 142.
(46) Weller, M. T.; Henry, P. F.; Wilson, C. C. *J. Phys. Chem. B* **2000**, *104*, 12224.

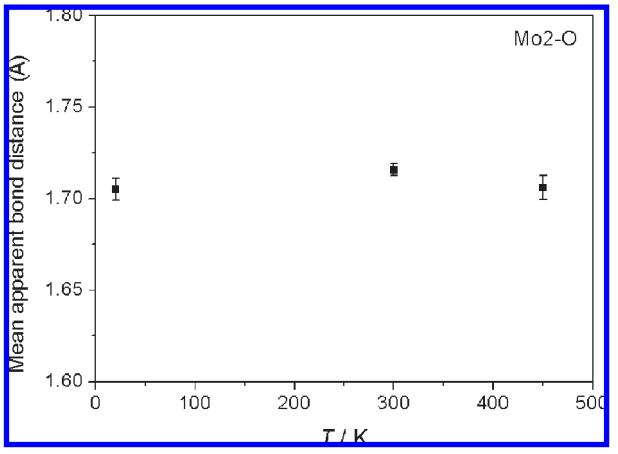

Figure 14. Mean apparent Mo2−O bond distances as a function of temperature for $Y_2Mo_3O_{12}$.

near-zero thermal expansion of stiff Mo−O bonds[47] and the existence of transverse vibrations of the oxygens (correlated motion of Y−O−Mo atoms).[48] Determinations of bond lengths can be affected in some situations by the real-space resolution of the diffraction experiment, here ~0.96 Å.[49] Precise determination of mean atomic positions for systems could be problematic where the atomic distribution is not a symmetrical function and/or where correlated motions of polyhedra exist, such that the calculated mean atomic position of the transverse vibrating atom is not the true midpoint of its atomic distribution. It could be suggested that a nonsymmetric atomic distribution and/or correlated motion are inherent for the oxygen atoms in $A_2M_3O_{12}$-type phases, resulting in an apparent decrease of the bond lengths involving oxygen atoms (Figure 6) and possible increase then decrease of bond lengths as a function of temperature, a feature exemplified by the apparent average Mo2−O bond (Figure 14), although more observations (for this and related materials) are needed to confirm trends. The reduction of the mean Y−Mo nonbonded distances and mean Y−O−Mo angles (Figure 8) with increasing temperature can be identified as the basic structural origin of negative thermal expansion of the unit-cell volume in $Y_2Mo_3O_{12}$.

5. Conclusions

Thermal properties of orthorhombic *Pbcn* $Y_2Mo_3O_{12}$, such as thermal expansion, stability and heat capacity, were investigated over a wide temperature range, as low as 2 K (heat capacity) and as high as 673 K (DSC). The orthorhombic-to-monoclinic phase transition, commonly observed in $A_2M_3O_{12}$ structures, is absent over the temperature range 2 to 673 K. In its orthorhombic *Pbcn* phase, $Y_2Mo_3O_{12}$ exhibited large negative thermal expansion ($\alpha_l = -9.02 \times 10^{-6}$ K^{-1}, averaged over $T = 20$ K to $T = 450$ K). The unit-cell parameter, *a*, shows anomalous behavior, increasing in the range between 20 and 300 K, then decreasing as the temperature is increased further. The latter is not due to a phase transition, but can be explained through a change of balance of atomic-level mechanisms contributing to expansion and reduction of interatomic distances. The inherent volume distortion parameter (v) of AO_6 has been introduced to quantitatively evaluate polyhedral distortion. This parameter is strongly correlated with the linear coefficient thermal expansion (α_l) of different members of the $A_2M_3O_{12}$ family; this correlation seems to be more robust than a previously proposed origin (A^{3+} ratio dictating thermal expansion) and can successfully explain the previously unresolved cases. It seems that the MO_4 tetrahedra also influence the thermal expansion properties of $A_2M_3O_{12}$ structures. Although the AO_6 and MO_4 polyhedra increase their distortion with increasing temperature, their distortion is two orders of magnitude lower than in ZrW_2O_8, in which ZrO_6 polyhedra are completely rigid. In conclusion, we find that the Y−Mo nonbonding distances and Y−O−Mo angles are the basic structural features that provoke negative thermal expansion in $Y_2Mo_3O_{12}$ and other isostructural compounds.

Acknowledgment. B.A.M. is grateful to the Brazilian Synchrotron Light Laboratory (LNLS) for the beam time and financial support under the project D10B-XPD 7756. M.A. thanks FAPERJ for financial support. M.A.W. acknowledges support from NSERC of Canada, along with the Canada Foundation for Innovation, Atlantic Innovation Fund, and other partners that fund the Facilities for Materials Characterization managed by the Institute for Research in Materials at Dalhousie University. We acknowledge H. Andreas, R. J. Boyd, and C. Whitman for useful discussions and comments.

Supporting Information Available: Phase transition temperatures of $A_2Mo_3O_{12}$ compounds; atomic positions for $Y_2Mo_3O_{12}$ at 20, 300, and 450 K; isotropic displacement factors for Y, Mo1, Mo2, and O; high-resolution XRPD patterns for $Y_2Mo_3O_{12}$ at 20 and 450 K adjusted through the Rietveld method; crystallographic information files (CIF) for 20, 300, and 450 K; volume distortion parameter (v) of ZrO_6 polyhedral as a function of temperature for ZrW_2O_8; calculated valences for Y^{3+}, W^{6+}, and O^{2-} as a function of temperature for $Y_2W_3O_{12}$; temperatures of the orthorhombic to monoclinic phase transitions in $A_2Mo_3O_{12}$ family as a function of the electronegativity of A^{3+} ions (Li-Xue scale); variations of individual Y−O and Mo1−O and Mo2−O bond lengths with temperature; experimental heat capacity data for $Y_2Mo_3O_{12}$ (different sample masses and thermal contact greases: Apiezon H and T). This material is available free of charge via the Internet at http://pubs.acs.org.

(47) Hazen, R. M.; Prewitt, C. T. *Am. Mineral.* **1977**, *62*, 309.
(48) Evans, J. S. O. *J. Chem. Soc., Dalton Trans.* **1999**, 3317.
(49) Tucker, M. G.; Dove, M. T.; Keen, D. A. *J. Phys.: Condens. Matter* **2000**, *12*, L425.